

# Advanced turning maneuver of a many-legged robot using pitchfork bifurcation

Shinya Aoi<sup>1</sup>, Ryoe Tomatsu<sup>1</sup>, Yuki Yabuuchi<sup>1</sup>, Daiki Morozumi<sup>1</sup>, Kota Okamoto<sup>1</sup>, Soichiro Fujiki<sup>2</sup>, Kei Senda<sup>1</sup>, and Kazuo Tsuchiya<sup>1</sup>

<sup>1</sup> Dept. of Aeronautics and Astronautics, Graduate School of Engineering, Kyoto University, Kyoto daigaku-Katsura, Nishikyo-ku, Kyoto 615-8540, Japan

<sup>2</sup> Dept. of Physiology and Biological Information, School of Medicine, Dokkyo Medical University, 880 Kita-Kobayashi, Mibu-machi, Shimotsuga-gun Tochigi 321-0293, Japan

**Abstract**—Legged robots have excellent terrestrial mobility for traversing diverse environments and thus have the potential to be deployed in a wide variety of scenarios. However, they are susceptible to falling and leg malfunction during locomotion. Although the use of a large number of legs can overcome these problems, it makes the body long and leads to many legs being constrained to contact with the ground to support the long body, which impedes maneuverability. To improve the locomotion maneuverability of such robots, the present study focuses on dynamic instability, which induces rapid and large movement changes, and uses a 12-legged robot with a flexible body axis. Our previous work found that the straight walk of the robot becomes unstable through Hopf bifurcation when the body axis flexibility is changed, which induces body undulations. Furthermore, we developed a simple controller based on the Hopf bifurcation and showed that the instability facilitates the turning of the robot. In this study, we newly found that the straight walk becomes unstable through pitchfork bifurcation when the body-axis flexibility is changed in a way different from that in our previous work. In addition, the pitchfork bifurcation induces a transition into a curved walk, whose curvature can be controlled by the body-axis flexibility. We developed a simple controller based on the pitchfork-bifurcation characteristics and demonstrated that the robot can perform a turning maneuver superior to that with the previous controller. This study provides a novel design principle for maneuverable locomotion of many-legged robots using intrinsic dynamic properties.

**Index Terms**—Many-legged robot, Maneuverability, Instability, Pitchfork bifurcation, Curved walk, Turning

## I. INTRODUCTION

LEGGED locomotion, such as that of animals, allows excellent terrestrial mobility for traversing diverse environments. Legged robots thus have potential to be deployed in a wide variety of scenarios, such as search and rescue [21], [35], hazardous environment operation and exploration [9], [51], and planetary exploration [6], [55]. Various legged robots with agile animal-like locomotion have recently been developed [1], [4], [23]–[25], [30], [33], [36], [37], [40], [46]. However, most of these robots have four legs and falling, which may result in the breakdown of mechanical and electrical components and from which it is difficult to recover, is inevitable during locomotion. Furthermore, damage to even one leg greatly degrades their locomotive performance [12]. The use of a large number of legs prevents falling and allows a certain level of leg malfunction to be tolerated [27], [34].

Although the use of a large number of legs has advantages for legged robots, it makes the body long and increases the difficulty of motion planning and control due to the many intrinsic degrees of freedom and complex interaction with the environment. In particular, many legs are physically constrained to be in contact with the ground to support the long body, which can impede maneuverability. While humans and quadrupeds lean their bodies to enhance turning maneuvers, the underlying mechanism of agile locomotion using a large number of legs remains unclear from biological and engineering viewpoints [18]. Thus, maneuverable locomotion for robots with a large number of legs remains challenging.

Conventional controllers precisely plan the motion of all degrees of freedom of the robot (e.g., how the long body is bent, where each foot touches the ground, and in what order the legs move) and control the robot to stabilize the desired motion. However, this approach has huge computational and energy costs, making it inefficient. To design a simple and efficient controller with high locomotor performance, the fundamental dynamic principles embedded in the robot dynamics, including the interaction with the environment, should be fully utilized [1], [10], [29], [30].

For maneuverable locomotion of many-legged robots that overcomes the above difficulties and the limitations of conventional approaches, the present study focuses on dynamic instability, which induces rapid and large movement changes, and uses a 12-legged robot whose body axis is flexible. Our previous work [2] showed that although many ground contact legs can impede maneuverability, they induce straight walk instability and body undulations through Hopf bifurcation when the body-axis flexibility is changed; bifurcation qualitatively changes a dynamical system by changing a parameter, and Hopf bifurcation changes the stability of an equilibrium point and creates a limit cycle [47]. Stability refers to the capability to resist and recover from disturbances; straight walk instability is thus expected to allow the robot to easily change walking direction. Therefore, we developed a simple controller based on the straight walk instability induced by the Hopf bifurcation to change walking direction without precise motion planning and control, and demonstrated that the straight walk instability facilitates the turning of the robot [3].

In the present study, we show that the pitchfork bifurcation

of the straight walk is caused by changes in the body-axis flexibility in a way different from that in previous work [2], [3]; pitchfork bifurcation changes the stability of an equilibrium point and creates two equilibrium points [47]. The pitchfork bifurcation not only destabilizes straight walking, but also causes curved walking, where the flexible body axis forms a curved shape. Furthermore, we found that the curvature of curved walking can be controlled by the body-axis flexibility. We developed a simple control strategy based on the pitchfork-bifurcation characteristics, which improved the turning maneuver compared to that achieved using Hopf bifurcation. This study also provides a design principle for a simple and efficient control scheme to create maneuverable locomotion for various robots using intrinsic dynamic properties.

## II. ROBOT

We used the many-legged robot developed in [2] and improved in [3]. The total length and mass are 135 cm and 8.5 kg, respectively. The robot consists of six body segment modules (modules 1–6), as shown in Fig. 1. Each module is composed of a single body and one pair of legs and has the same length. The body segments are passively connected by yaw joints (yaw joints 1–5) in which torsional springs (the spring constant is  $k_i$  ( $i = 1, \dots, 5$ )) and potentiometers are installed at the axes. The yaw joint angles are zero when the body segments are aligned. Each leg has two links connected by pitch joints. The legs in the first module (module 1) have an additional link connected by a yaw joint to supplement the control of the walking direction during turning tasks. Each leg joint is manipulated by an encoder-equipped motor. The first module has a laser range scanner with a viewing angle of 240 deg (Hokuyo, URG-04LX) to find the relative position of a target for turning. The robot was controlled by an external host computer (Intel Pentium 4 2.8 GHz, RT-Linux) with 2-ms intervals, and walked on a flat wooden floor with a vinyl floor mat to suppress slipping. The computer control signals and electric power were provided via external cables, which were kept slack and suspended to avoid influencing the locomotor behavior of the robot.

To make the robot walk in a straight line, we controlled the legs using the two pitch joints of each leg to follow the desired movement, which consists of two parts, namely half of an elliptical curve that starts from the posterior extreme position (PEP) and ends at the anterior extreme position (AEP), and a straight line from the AEP to the PEP (Fig. 1B). In the straight line, the leg tips moved from the AEP to the PEP at a constant speed parallel to the body. We set the duration of the half elliptical curve to 0.29 s, that of the straight line to 0.31 s, and the distance between the AEP and the PEP in each leg to 3 cm. The left and right legs in each module moved in antiphase, and the relative phase between the ipsilateral legs on adjacent modules was set to  $2\pi/3$  rad. When the leg yaw joint angles of the first module were fixed so that the leg tip trajectories were parallel to the body, the robot was expected to walk in a straight line while keeping the body segments parallel to each other because torsional springs were installed on the body-segment yaw joints and all support-leg tips moved parallel to the body segments at an identical speed.

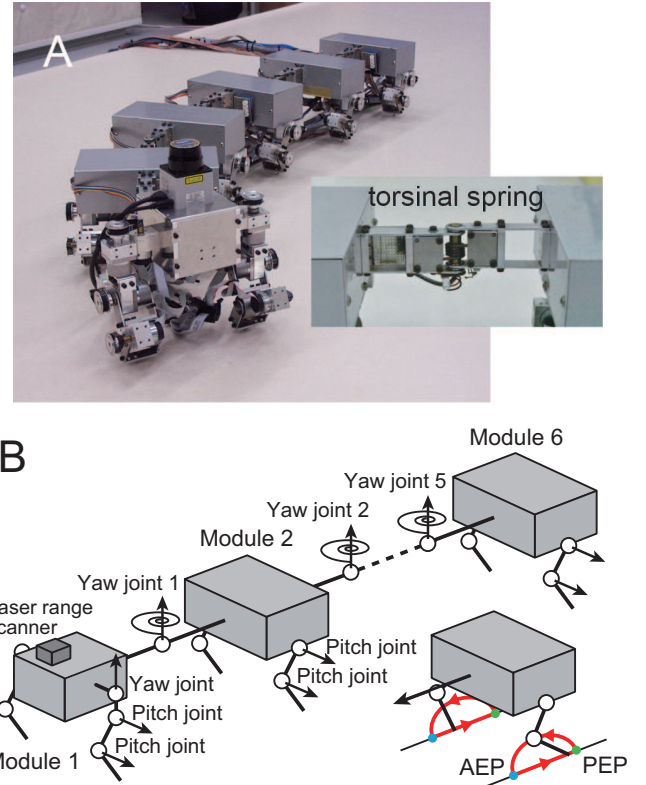


Fig. 1. (A) Photograph and (B) schematic model of many-legged robot. The robot consists of six modules, each of which has one body segment and one pair of legs. The legs are controlled by two pitch joints so that the leg tips follow a periodic trajectory, including the anterior extreme position (AEP) and the posterior extreme position (PEP). Body segments are passively connected by yaw joints with installed torsional springs. The legs in the first module have additional yaw joints to change the walking direction. A laser range scanner is installed on the first module to find a position relative to a target.

## III. PITCHFORK BIFURCATION OF STRAIGHT WALK

### A. Experimental results

Our previous work [2], [3] revealed that when we used torsional springs with the same spring constant for all body-segment yaw joints (yaw joints 1–5) and changed the spring constant uniformly among the joints, the straight walk became unstable through Hopf bifurcation, which induced body undulations. This bifurcation was verified by a Floquet analysis, which investigates the stability of solutions of linear differential equations with periodic coefficients, with a simple physical model. In this study, we performed robot experiments of walking in a straight line, where we changed the body-axis flexibility in a way that was different from that in our previous work. Specifically, we used the same torsional spring for yaw joints 2–5 with  $k_i = 41$  Nmm/deg ( $i = 2, \dots, 5$ ) and various torsional springs for yaw joint 1 with  $k_1 = 15, 17, 21, 28, 41,$  and  $75$  Nmm/deg. We set all the body segments parallel to each other as the initial conditions. The leg yaw joints in the first module were fixed during the experiments and we did not attempt to control the walking direction, that is, the walking direction was an open loop.

When we used large spring constants for  $k_1$ , the robot kept walking in a straight line as expected, and the body segments

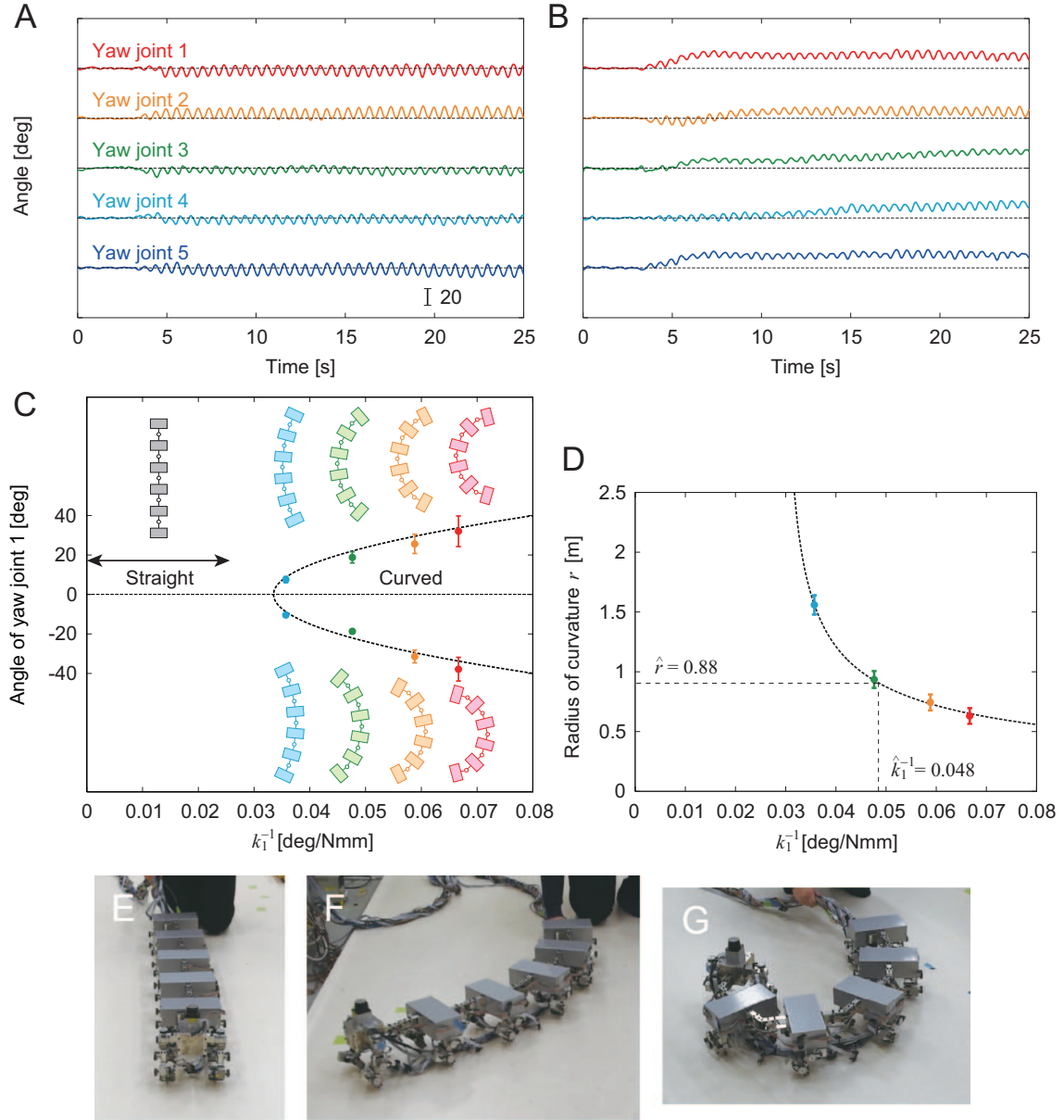


Fig. 2. Characteristics of curved walk for  $k_1$  values below the threshold value. Yaw joint angles for (A) straight walk with  $k_1 = 41$  Nmm/deg and (B) curved walk with  $k_1 = 15$  Nmm/deg (see Movie 1). (C) Average angle of yaw joint 1 during curved walk for  $1/k_1$  that indicates pitchfork bifurcation. The data points and error bars correspond to the means and standard errors, respectively, of the results of five experiments. (D) Radius of curvature of body axis for  $1/k_1$ . The data points and error bars correspond to the means and standard errors, respectively, of the results of 10 experiments. Photographs of (E) straight walk with  $k_1 > \hat{k}_1$ , (F) curved walk with small curvature with  $k_1 \sim \hat{k}_1$ , and (G) curved walk with large curvature with  $k_1 < \hat{k}_1$ .

were aligned, with all body-segment yaw joint angles being almost zero (Figs. 2A and E, see Movie 1). However, when  $k_1$  was set to below a threshold value, the body-segment yaw joints showed non-zero angles with the same sign; that is, the body axis was curved and the robot walked in a curved line (Figs. 2B, F, and G, see Movie 1). Specifically, the robot walked in a curved line for  $k_1 = 15, 17, 21,$  and  $28$  Nmm/deg, but not for  $k_1 = 41$  and  $75$  Nmm/deg. Furthermore, both left- and right-curved walking appeared. Figure 2C shows the angles of yaw joint 1 for  $1/k_1$  averaged over 5 s during a curved walk (the angles for the other body-segment yaw joints are shown in Fig. 3). Although the angles slightly

differ among yaw joints 1–5 partly due to feet slippage, these data indicate that the body axis shows a curved shape. Furthermore, while the fluctuation among the trials increases with  $1/k_1$ , the magnitude of these angles increases with  $1/k_1$ . These results suggest that the presence of pitchfork bifurcation depends on  $k_1$ . These angle data were fitted by the square root of  $1/k_1$  [47]. The bifurcation point was estimated to be  $k_1 = 34$  Nmm/deg ( $1/k_1 = 0.030$  deg/Nmm).

The dependence of the body-segment yaw joint angles on  $1/k_1$  (Fig. 2C and Fig. 3) indicates the change of the curved shape of the body axis for the curved walk. Figure 2D shows the radius of curvature  $r$  of the body axis for  $1/k_1$  calculated

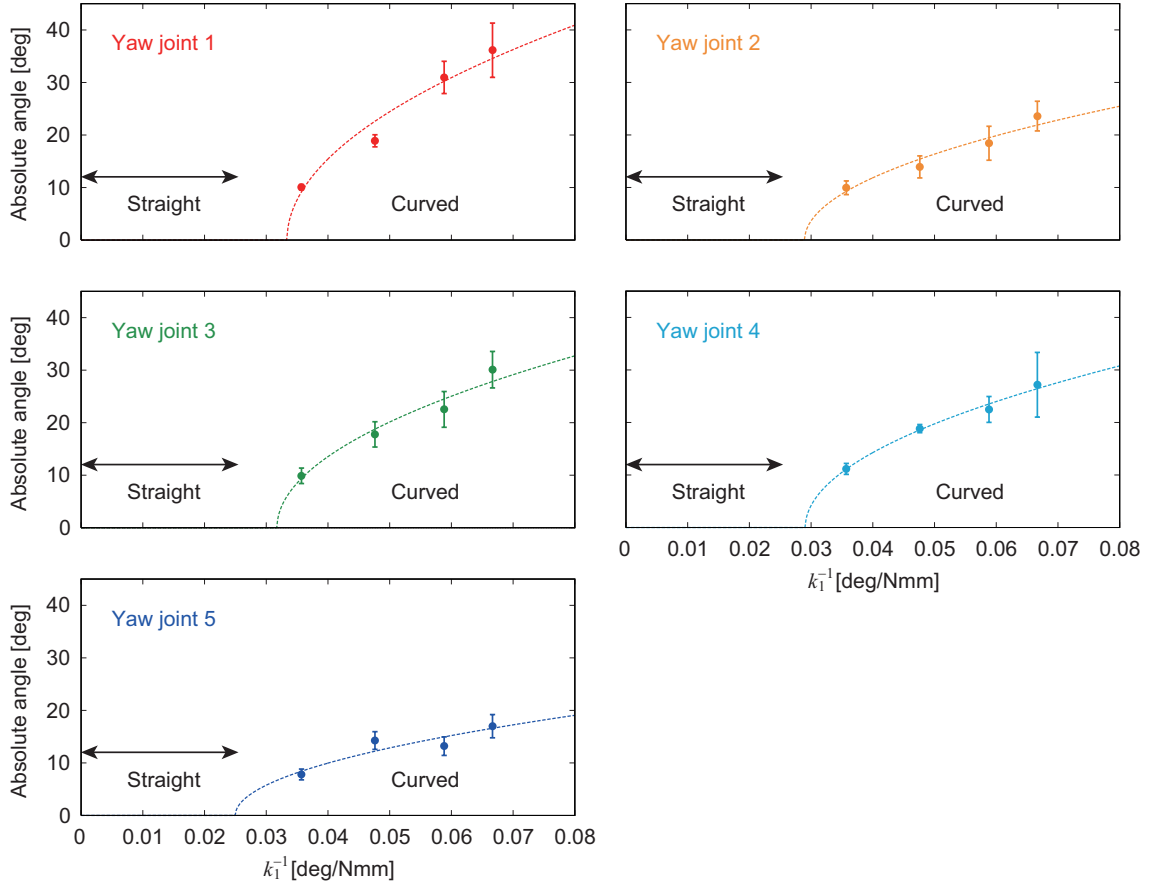


Fig. 3. Average absolute angles of body-segment yaw joints during curved walk for  $1/k_1$ . The data points and error bars correspond to the means and standard errors, respectively, of the results of 10 experiments.

as  $r = 5L / \sum_{i=1}^5 |\theta_i|$ , where  $\theta_i$  is the angle of yaw joint  $i$  ( $i = 1, \dots, 5$ ) and  $L$  is the length of the body segments. This figure shows that we can control the curvature of the body axis to perform a curved walk by adjusting  $k_1$  through pitchfork bifurcation.

The pitchfork bifurcation also depends on parameters other than  $k_1$ . To investigate this, we used different values for the spring constant of yaw joints 2–5, gait speed, and relative phase between the ipsilateral legs on adjacent modules. Specifically, we changed  $k_{2-5}$  from 41 to 28 Nmm/deg, the distance between the AEP and the PEP in each leg (Fig. 1B) from 3 to 1.8 cm, or the relative phase from  $2\pi/3$  to  $\pi$ , and performed the same experiments shown in Fig. 2. As a result, these values also induced a curved walk below a critical value of  $k_1$ . However, the estimated bifurcation point and radius of curvature of the body axis changed as shown in Fig. 4. Specifically, when the spring constant of yaw joints 2–5 and gait speed decreased, the estimated bifurcation point decreased from  $k_1 = 34$  to 23 and 25 Nmm/deg ( $1/k_1 = 0.030$  to 0.043 and 0.040 deg/Nmm), respectively. However, the radius of curvature remained almost unchanged. In contrast, while the relative phase did not change the bifurcation point as much ( $k_1 = 31$  Nmm/deg,  $1/k_1 = 0.032$  deg/Nmm), it achieved a smaller radius of curvature.

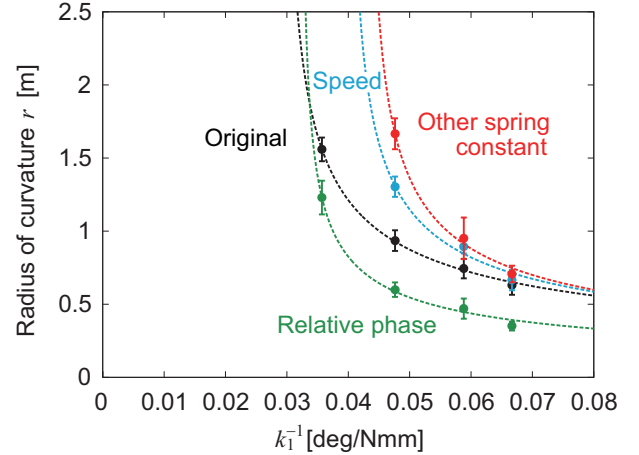


Fig. 4. Change in radius of curvature by different values for the spring constant of yaw joints 2–5, gait speed, and relative phase between the ipsilateral legs on adjacent modules. The data points and error bars correspond to the means and standard errors, respectively, of the results of five experiments.

#### B. Verification by Floquet analysis with simple physical model

The robot experiments suggested that the presence of pitchfork bifurcation in the straight walk depends on the spring constant  $k_1$  (Figs. 2C, 3, and 4). We verified this bifurcation



from a theoretical viewpoint using a Floquet analysis with a simple physical model, as done in our previous work [2]. The model was simplified from the original high-dimensional mechanical model to extract the fundamentals of locomotion dynamics (Fig. 5A). In particular, the model was two-dimensional because the movements were designed to make the robot walk without up-and-down, roll, or pitch motions of the body segments. Furthermore, because an important role of legs in locomotion is to receive reaction forces from the floor, we neglected the inertial force of the legs and instead modeled the reaction forces at the leg tips based on the geometric conditions. Specifically, we assumed that the leg tips move relative to the body segments as designed and that the leg tips receive the friction forces during the straight line from the AEP to the PEP (Fig. 1B), which are proportional to the velocities relative to the floor.

The equations of motion of the simple model can be expressed as

$$K(q)\ddot{q} + h(q, \dot{q}) = u(q, \dot{q}) + \lambda(q, \dot{q}, t) \quad (1)$$

where  $q = [xy\theta_0 \cdots \theta_5]^T$ ,  $[xy]$  and  $\theta_0$  are the position and yaw angle of the first module, respectively;  $K(q)$  is the inertia matrix;  $h(q, \dot{q})$  is the nonlinear term;  $u(q, \dot{q})$  is the torque term of the torsional springs; and  $\lambda(q, \dot{q}, t)$  is the reaction force term. Because the leg tips move periodically relative to the body segments, the reaction force  $\lambda$  becomes a function of time  $t$ . The detailed description and derivation of the equations of motion (1) are shown in our previous work [2]. During the straight walk of the model, we can write  $\dot{q} = [vt + x_0 y_0 0 \cdots 0]^T$  and  $\hat{q} = [v 0 0 \cdots 0]^T$ , where  $x_0$  and  $y_0$  represent the initial position of the first module and  $v$  is the velocity of the leg tips relative to the body segments. For  $z^T = [q^T \hat{q}^T]$ , the linearization of the equations of motion (1) for a straight walk using  $z = \hat{z} + \delta z$  gives

$$\delta \dot{z} = A(t)\delta z \quad (2)$$

Because the movements of the leg tips are periodic with the gait cycle  $\tau$ ,  $A(t + \tau) = A(t)$  is satisfied. The detailed description and derivation of the linearized equation (2) are also shown in our previous work [2]. The fundamental solution matrix  $Z(t)$  of the linearized equation with periodic coefficients (2) can be expressed as

$$Z(t) = \Phi(t)e^{\Lambda t} \quad (3)$$

where  $\Phi(t + \tau) = \Phi(t)$  [19]. Because we can use an identity matrix for  $Z(0)$  and  $\Phi(0)$ , the integration of (2) from  $t = 0$  to  $\tau$  yields

$$Z(\tau) = \Phi(\tau)e^{\Lambda\tau} = \Phi(0)e^{\Lambda\tau} = e^{\Lambda\tau} \quad (4)$$

The Floquet exponents (eigenvalues of the constant matrix  $\Lambda$ ) and corresponding eigenvectors explain the behavior of the model. Specifically, when all real parts of the exponents are negative, the straight walk of the model is asymptotically stable. In contrast, if any real part of the exponents is positive, the straight walk becomes unstable. In our previous work [2], when all the spring constants of yaw joints 1–5 of the simple model were decreased uniformly, one pair of the Floquet exponents crossed the imaginary axis from the left-half plane and

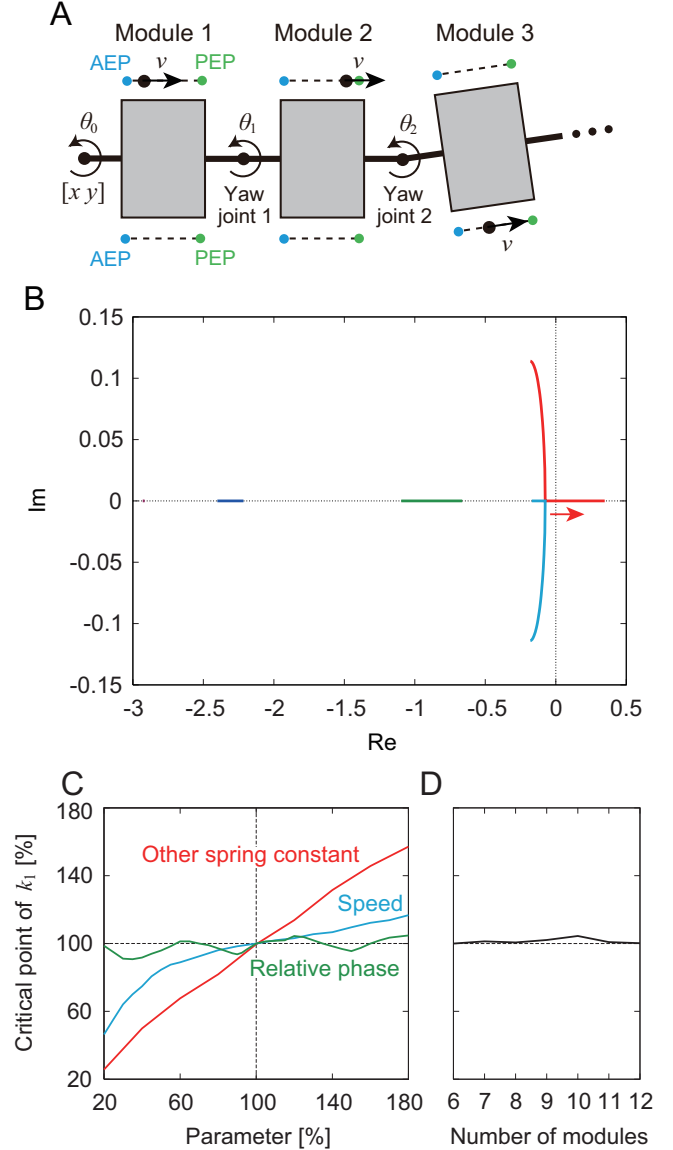


Fig. 5. Floquet analysis using simple two-dimensional model. (A) Simple model. (B) Floquet exponents when  $k_1$  was varied. Different colors represent different exponents. The exponent in red crosses into the right-half plane along the real axis, indicating pitchfork bifurcation. The change in critical value of  $k_1$  by (C) spring constant of yaw joints 2–5, gait speed, and relative phase between the ipsilateral legs on adjacent modules, and (D) number of modules.

entered the right-half plane above a critical value of the spring constant, which indicates an oscillatory destabilization of the straight walk to produce body undulations and implied Hopf bifurcation (strictly speaking, this corresponds to Neimark-Sacker bifurcation when considering the periodicity of the gait cycle [26]). Furthermore, the relative amplitude and phase between the components of the destabilizing eigenvector were comparable to those of the yaw joint movements during the robot experiments. The Floquet analysis using a simple model is useful for verifying the bifurcation observed in the robot experiments.

Figure 5B shows the Floquet exponents of the simple model when  $k_1$  was varied while the other spring constants  $k_i$  ( $i = 2, \dots, 5$ ) remained fixed, as done in the robot

experiments. Except for the zero exponents, all exponents lie in the left-half plane for large  $k_1$ . However, with decreasing  $k_1$ , one exponent moves along the real axis and enters the right-half plane above  $k_1 = 12$  Nmm/deg. Although this critical value is smaller than the bifurcation point estimated in the robot experiments in Section III-A, the components of the destabilizing eigenvector for yaw joints 1–5 at the critical point were 0.64, 0.36, 0.48, 0.46, and 0.16, respectively, showing the same sign. This indicates that the straight walk is destabilized to produce a curved walk (positive disturbance induces right-curved walk and negative disturbance induces left-curved walk) and implies pitchfork bifurcation. Furthermore, the ratio between the components of the destabilizing eigenvector is consistent with the ratio between the yaw joint angles during the curved walk of the robot experiments (Fig. 3). Although this analysis does not estimate the radius of curvature after the bifurcation due to the limitation of the linear analysis, these results verify the destabilization of the straight walk and the emergence of a curved walk through pitchfork bifurcation, as observed in the robot experiments.

We also investigated the parameter dependence of the pitchfork bifurcation. Figure 5C shows how the critical value of  $k_1$  changes as the spring constant of yaw joints 2–5, gait speed, and relative phase between the ipsilateral legs on adjacent modules change in the same way as in the robot experiments in Fig. 4. In addition, Fig. 5D shows the change in the critical value when the number of the body segments is increased. When the spring constant of yaw joints 2–5 and gait speed decrease, the critical value decreases. However, the relative phase does not change the critical value as much. These results are consistent with those in the robot experiments (Fig. 4). The number of body segments also does not change the critical value very much. Although we investigated the effects of only changes in the spring constant of yaw joints 2–5, gait speed, relative phase, and number of body segments, this Floquet analysis can investigate other parameters, such as the length and mass, as performed in our previous work [2] for Hopf bifurcation.

#### IV. TURNING MANEUVERABILITY

##### A. Turning strategy based on pitchfork bifurcation

To investigate the maneuverability of the robot achieved with the aid of pitchfork bifurcation, we focused on a turning task in which the robot approached a target located on the floor in a direction different from that to which the robot was oriented, as performed in our previous work [3], which investigated the maneuverability with the aid of Hopf bifurcation. For a target at any location (relative angle  $\psi$  and distance  $R$ ), there exists a unique radius of curvature  $\hat{r}$  of the curved walk with which the robot will approach the target (Fig. 6A). Because the radius of curvature  $r$  of the body axis induced by the pitchfork bifurcation monotonically decreases with  $1/k_1$  (Fig. 2D),  $k_1 = \hat{k}_1$  is uniquely determined so that  $r = \hat{r}$ . This means that when we use  $k_1 = \hat{k}_1$ , the robot spontaneously approaches the target due to the pitchfork bifurcation characteristics, which is an optimal strategy for turning. However, this strategy is feedforward, depending on

the initial conditions of the robot and target, that is, an open loop for the walking direction. In particular, the direction in which the robot turns (left or right) depends on the initial robot conditions because of the pitchfork bifurcation characteristics, and thus this strategy does not guarantee the success of the turning tasks. Therefore, we also used a supplementary turning controller developed in our previous work [3], which uses the laser range scanner of the first module to measure the relative target angle and manipulates the leg yaw joints of the first module to approach the target based on the measured target angle (see Appendix B). This supplementary controller is a closed loop for the walking direction and allows the robot to approach the target even when  $k_1 \neq \hat{k}_1$ .

##### B. Experimental results

For the initial conditions, we used  $\psi = 45^\circ$  and  $R = 1.3$  m for the relative angle and distance between the first module and the target, respectively, which yielded  $\hat{r} = 0.88$  m and  $\hat{k}_1 = 21$  Nmm/deg ( $1/\hat{k}_1 = 0.048$  deg/Nmm), and set all body-segment yaw joint angles to zero (Fig. 6F). Figure 6B shows the trajectory of the first module on the floor during the turning task for three torsional spring constants, namely  $k_1 = 15$  ( $< \hat{k}_1$ ),  $21$  ( $\sim \hat{k}_1$ ), and  $41$  Nmm/deg ( $> \hat{k}_1$ ). Figures 6C and D show the time profiles of the target distance and relative target angle with respect to the walking direction, respectively, for these three spring constants. When the distance was less than 0.15 m, we assumed that the robot reached the target and this task was successfully completed. For  $k_1 = 41$  Nmm/deg ( $> \hat{k}_1$ ), the robot hardly changed walking direction and the first module trajectory bulged outward. As a result, the robot could not reach the target (Fig. 6G, see Movie 2). For  $k_1 = 15$  Nmm/deg ( $< \hat{k}_1$ ), although the robot could quickly change walking direction, it moved in directions away from the target due to the small radius of curvature created by pitchfork bifurcation and could not reach the target (Fig. 6I, see Movie 2). In contrast, for  $k_1 = 21$  Nmm/deg ( $\sim \hat{k}_1$ ), the robot reached the target through the optimal curved walk generated by pitchfork bifurcation (Fig. 6H, see Movie 2).

To quantitatively clarify the turning performance dependence on  $k_1$ , we employed three evaluation criteria, namely  $\varepsilon_1$ ,  $\varepsilon_2$ , and  $\varepsilon_3$ . For the criterion  $\varepsilon_1$ , we used the distance of the target at 23 s (the earliest time at which the task is successfully completed) to evaluate how quickly and successfully the robot approached the target. For the criterion  $\varepsilon_2$ , we used the absolute value of the relative target angle with respect to the walking direction at 23 s to evaluate how quickly and successfully the robot was oriented to the target. For the criterion  $\varepsilon_3$ , we used the amount of the control input during the task from the supplementary turning control in the leg yaw joints of the first module (Appendix B) to evaluate how efficiently the robot performs turning. Specifically,  $\varepsilon_3 = \int (\dot{\psi}_1^2 + \dot{\psi}_2^2) dt$ . Figure 6E shows the results for  $1/k_1$ . All criteria showed minimum values around  $k_1 = \hat{k}_1$ , which means that the turning strategy using pitchfork bifurcation achieved the best performance and that the robot made the best use of the curved walk induced by pitchfork bifurcation to complete the turning task.

To verify the performance of the proposed controller using pitchfork bifurcation, we additionally performed the same ex-

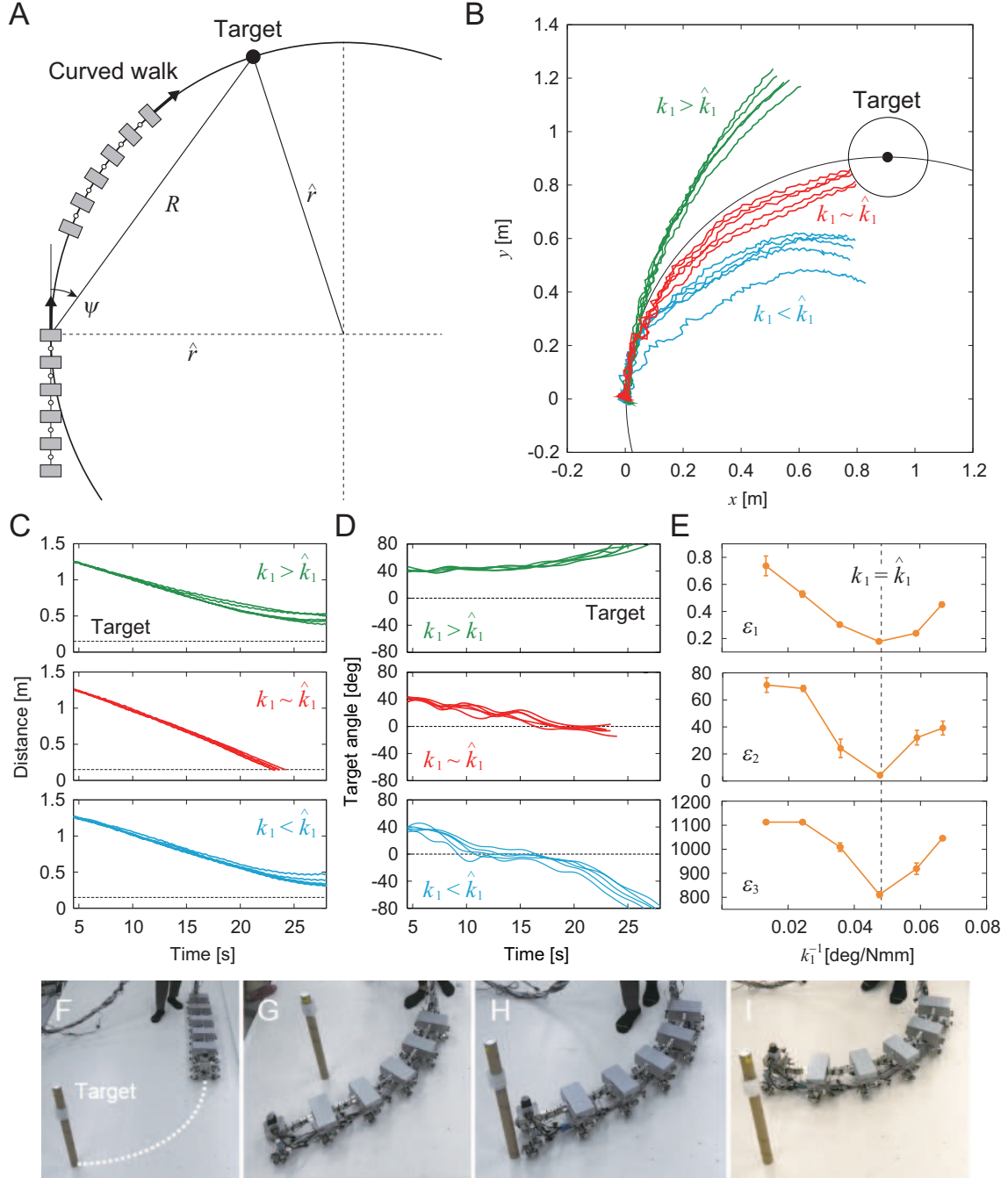


Fig. 6. Turning task. (A) Radius of curvature  $\hat{r}$  of curved walk with which the robot approaches a target (relative angle  $\psi$  and distance  $R$ ). (B) Trajectory of the first module on the floor, (C) target distance, and (D) relative target angle for five experiments for three spring constants with  $\psi = 45^\circ$ ,  $R = 1.3$  m,  $\hat{r} = 0.88$  m, and  $1/\hat{k}_1 = 0.048$  deg/Nmm (see Movie 2). (E) Evaluation criteria  $\varepsilon_1$ ,  $\varepsilon_2$ , and  $\varepsilon_3$  for  $1/k_1$ . The data points and error bars correspond to the means and standard errors, respectively, of the results of five experiments. Photographs of (F) initial conditions, (G) unsuccessful approach with  $k_1 > \hat{k}_1$ , (H) successful approach with  $k_1 \sim \hat{k}_1$ , and (I) unsuccessful approach with  $k_1 < \hat{k}_1$ .

periment as that in Fig. 6B but using different initial conditions of the target, namely  $\psi = 40^\circ$  and  $R = 1.5$  m, which yielded  $\hat{r} = 1.2$  m and  $\hat{k}_1 = 26$  Nmm/deg ( $1/\hat{k}_1 = 0.039$  deg/Nmm). Figures 7A, B, and C show the evaluation criteria  $\varepsilon_1$ ,  $\varepsilon_2$ , and  $\varepsilon_3$ , respectively, for  $1/k_1$ . All criteria show minimum values around  $k_1 = \hat{k}_1$ , which means that the turning strategy using pitchfork bifurcation achieved the best performance, in the same way as shown in Fig. 6E. The results show similar trends, which verifies the performance of the proposed controller.

### C. Contribution of supplementary turning control

As demonstrated above, the robot achieved maneuverable and efficient turning to approach a target using the curved walk induced by the pitchfork bifurcation. However, when the robot starts the approach with the body axis straight, it takes some time for the convergence to a curved walk, as shown in Fig. 2B. In addition, because the initial straight walk corresponds to the unstable solution of the pitchfork bifurcation, it is unclear whether the robot will turn to the

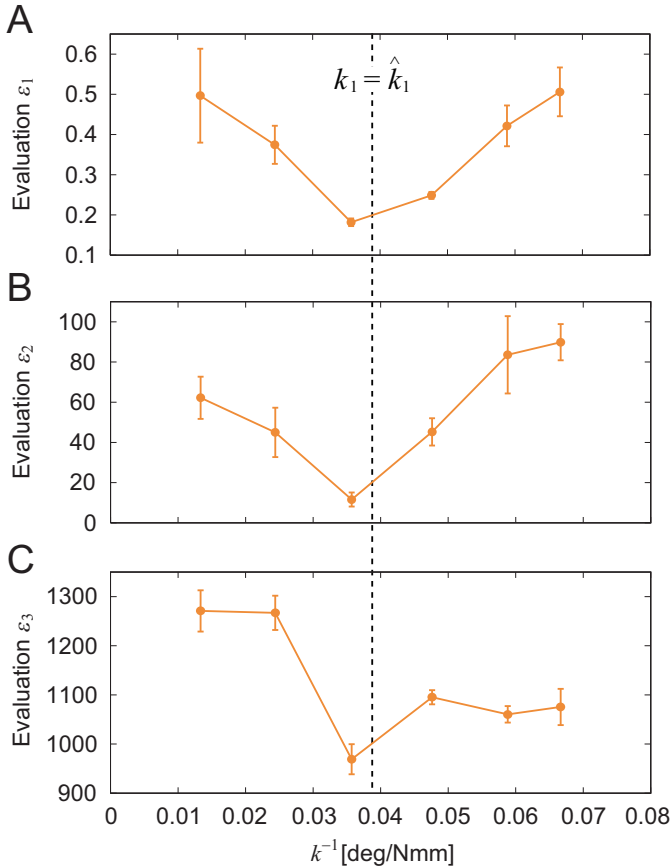


Fig. 7. Evaluation criteria (A)  $\varepsilon_1$ , (B)  $\varepsilon_2$ , and (C)  $\varepsilon_3$  for  $1/k_1$  for different conditions ( $1/\hat{k}_1 = 0.039$  deg/Nmm). The data points and error bars correspond to the means and standard errors, respectively, of the results of five experiments.

left or right, as shown in Fig. 2C (the disturbance determines the turning direction and the robot continues walking straight unless disturbed). Because the use of the optimal spring constant  $\hat{k}_1$  does not necessarily guarantee the success of the approach to the target, we also used the supplementary turning controller in the leg yaw joints in the first module.

To clarify the contribution of this supplementary controller, we also performed experiments without using the supplementary controller for  $k_1 = 21$  Nmm/deg ( $\sim \hat{k}_1$ ). The experimental conditions were identical to those in Fig. 6B. Figure 8 compares the trajectory of the first module on the floor during the turning task with and without the supplementary controller. In all the trials with the supplementary controller, the robot successfully approached the target. In contrast, the robot without the supplementary controller failed in many trials, because the robot started walking in a straight line and took some time to converge to walking in a curved line, and it sometimes curved to the different direction from the target, as expected.

#### D. Comparison with previous strategy

To examine how the turning performance was improved by pitchfork bifurcation, we also performed experiments using the turning strategy based on Hopf bifurcation used in our previous

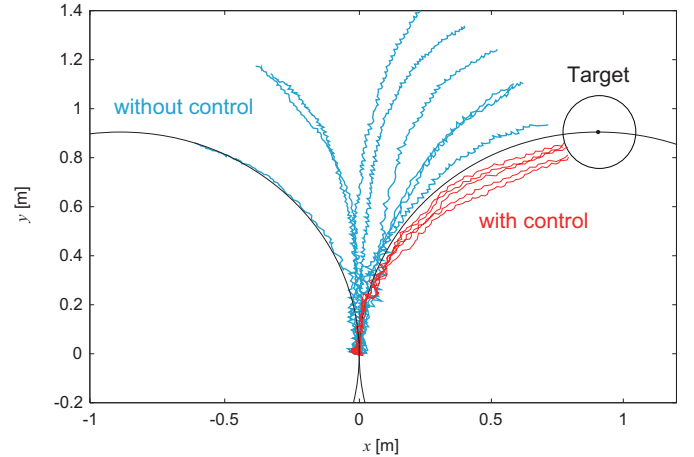


Fig. 8. Comparison of the trajectory of the first module on the floor during the turning task with and without the supplementary turning controller. Nine trials without the supplementary controller and five trials with the controller (Fig. 6B) are shown.

work [3] and compared the performance. For Hopf bifurcation, we used the same spring constant among the body-segment yaw joints and employed five spring constants ( $k_i = 8.7, 11, 15, 21, \text{ and } 41$  Nmm/deg,  $i = 1, \dots, 5$ ) to evaluate the turning performance for  $k_i$ , where the Hopf bifurcation point is about  $k_i = 18$  Nmm/deg ( $1/\hat{k}_i = 0.057$  deg/Nmm), as obtained in our previous work [3]. The experimental conditions were identical to those in Fig. 6E except for the spring constants of the body-segment yaw joints. Figures 9A, B, and C compare the turning performance in terms of the criteria  $\varepsilon_1$ ,  $\varepsilon_2$ , and  $\varepsilon_3$ , respectively, between the strategies based on pitchfork and Hopf bifurcations. All criteria for Hopf bifurcation showed minimum values in the unstable region, as observed in our previous work [3]. However, the minimum values of pitchfork bifurcation are lower than those of Hopf bifurcation for all criteria. This means that the turning strategy based on pitchfork bifurcation created by tuning the body-axis flexibility is superior to that based on Hopf bifurcation, which was developed in our previous work [3].

## V. CONCLUSION AND DISCUSSION

In this study, we found that the straight walk of a many-legged robot with flexible body axis becomes unstable through pitchfork bifurcation when the body-axis flexibility is changed. The straight walk transitioned into curved walk, whose curvature depended on the body-axis flexibility. We developed a simple controller based on the pitchfork-bifurcation characteristics and demonstrated that the robot achieves high turning maneuver superior to the previous controller based on the Hopf bifurcation.

Maneuverability is related to the ability to change movement direction. When the movement direction is destabilized during locomotion, the instability provides driving forces to rapidly change the movement direction and thus enhances maneuverability. Some military aircraft, such as the F-16, are designed to be aerodynamically unstable to enhance maneuver-



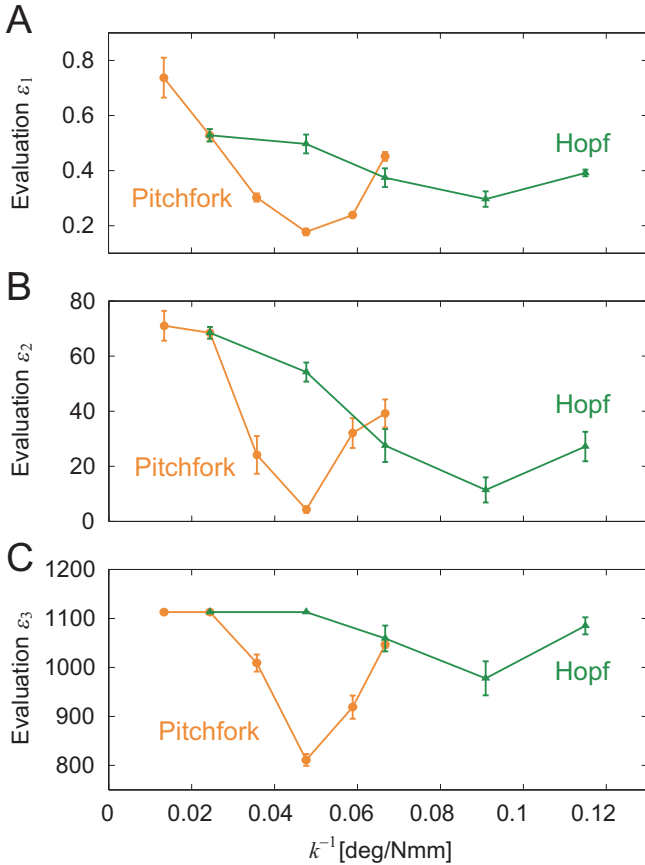


Fig. 9. Comparison of evaluation criteria (A)  $\varepsilon_1$ , (B)  $\varepsilon_2$ , and (C)  $\varepsilon_3$  between the turning strategies based on pitchfork bifurcation and Hopf bifurcation. The data points and error bars correspond to the means and standard errors, respectively, of the results of five experiments.

ability [8], [28]. The use of dynamic instability is thus useful from an engineering viewpoint.

The strategy of using movement direction instability to enhance maneuverability is also used by animals. Because the instability is determined by the body dynamics during interaction with the environment, it is prominent in locomotion generated through aerodynamics and hydrodynamics, such as the locomotion of flying insects [15], [38], [49] and sea animals [16], [17], [53]. It also appears in legged locomotion. When the center of mass is high, as in mammals, whose legs are under the body, leaning the body to the left or right induces instability and helps turning [11], [42]. However, when the center of mass is low, as in reptiles and arthropods, whose legs are away from the side of the body, locomotor behavior is almost two-dimensional because the center of mass moves in a horizontal plane. Therefore, the effect of body leaning is small and thus such a turning strategy cannot be used, which implies that the stability of the walking direction in the horizontal plane becomes more crucial. It has been suggested that cockroaches manipulate the position of the reaction forces from the floor entering the body to control the stability of a straight walk in a horizontal plane and that the straight walk instability helps their turning [39], [42].

Various bioinspired robots that use their body axis for

propulsion, such as snake robots [7], [45] and fish robots [13], [31], [43], have high maneuverability. However, legged robots still have difficulty in achieving highly maneuverable locomotion. This is partly because their interaction with the environment (i.e., foot contact with the ground) is intermittent due to the repetition of foot-contact and foot-off phases in leg movement. Although this intermittency allows the traversal of diverse environments, it can make the robot lose balance. Therefore, the control design of legged robots has focused on the avoidance of balance loss using dynamic criteria, such as a supporting polygon [20] and a zero-moment point [52], and maneuverability has not been well investigated. Although increasing the number of legs prevents balance loss, it also increases the number of contact legs, which impedes maneuverability. Moreover, the number of degrees of freedom to be controlled increases, making both motion planning and control difficult. In addition, many-legged robots generally use actuators for controlling not only the leg joints but also body-segment joints [48], [54], which requires huge computational and energy costs. In contrast, our robot has passive body-segment joints, which do not directly control the movement of the body axis, and instead determines the body-axis flexibility to induce a curved walk by the pitchfork bifurcation in the robot dynamics. The generation of robot movements with dynamics rather than actuators is crucial for efficient locomotion [10], and our strategy greatly reduces the computational and energy costs. Both the pitchfork and Hopf bifurcations induce the straight walk instability and thus contribute to the maneuverability. However, because the pitchfork bifurcation causes a curved walk used for turning, unlike the Hopf bifurcation that causes body undulations, the pitchfork bifurcation makes a greater contribution. Furthermore, when such bifurcation is introduced into the locomotion dynamics of other robots, such as snake and fish robots, through the mechanical and control design, it would contribute to improving their maneuverability.

In the present study, we investigated the contribution of the pitchfork bifurcation to maneuverability in robot experiments where the robot performs turning only once on a flat floor. It is important to clarify the contribution of the pitchfork bifurcation in more complex scenarios and environments in the future. In particular, consecutive turnings are crucial for complex scenarios. However, when we consider the experiments where the robot sequentially approaches multiple targets placed at different locations on the floor, that is, the robot performs multiple consecutive turnings, the initial conditions of the targets, such as the relative angle and distance, will differ in each turning. Different initial conditions of the targets induce different radiuses of curvature for optimal turning, which require different body-axis flexibilities. Because our robot uses torsional springs to determine the body-axis flexibility, it is impossible to change the flexibility during the experiment. In future studies, we would like to improve our robot and controller, for example, by incorporating a variable flexibility mechanism in the body axis to conduct more complex tasks. In addition, various turning strategies have been developed in quadruped and hexapod robots to modulate the leg movements for turning using bioinspired approaches based on central

pattern generators and sensory systems [5], [22], [32], [44], [50], [57] and optimization techniques [14], [41], [56]. We would like to improve our instability-based strategy in the body axis movement based on these strategies to enhance turning maneuverability of multi-legged robots in the future.

#### APPENDIX A SUPPLEMENTARY MOVIES

We recorded two supplementary movies to show the pitchfork bifurcation of a straight walk and turning performance in the robot experiments:

Movie 1: Straight walk, curved walk with a small curvature, and curved walk with a large curvature using a large spring constant, small spring constant, and very small spring constant, respectively, for the torsional spring in yaw joint 1.

Movie 2: Unsuccessful approaches using a spring constant larger and smaller than the optimal value for yaw joint 1, and successful approach using a spring constant close to the optimal value.

#### APPENDIX B SUPPLEMENTARY TURNING CONTROL BY LEG JOINTS

The optimal turning strategy is feedforward, depending only on the initial relative position between the robot and target. In addition, the direction in which the robot turns (left or right) depends on the initial robot conditions because of the property of pitchfork bifurcation. To guarantee a successful approach to the target, we used a supplementary feedback-based turning controller, which was developed in our previous work [3]. Specifically, we used the relative target angle  $\psi$  of the first module measured by the laser range scanner and the leg yaw joints  $\psi_1$  and  $\psi_2$  of the first module. We determined the desired angles  $\hat{\psi}_1$  and  $\hat{\psi}_2$  of  $\psi_1$  and  $\psi_2$  for each gait cycle [ $t_i^n \leq t < t_i^n + T$ , where  $t = t_i^n$  is the time when the desired leg tip is at the PEP for the  $n$ th gait cycle, and  $T$  is the gait cycle duration (= 0.6 s)] using

$$\hat{\psi}_i(t) = \begin{cases} \hat{\psi}_i(t_i^n) & t_i^n \leq t < t_i^n + t_{\text{start}} \\ \hat{\psi}_i(t_i^n) + \Delta_i \frac{t - t_i^n - t_{\text{start}}}{t_{\text{end}} - t_{\text{start}}} & t_i^n + t_{\text{start}} \leq t \leq t_i^n + t_{\text{end}} \\ \hat{\psi}_i(t_i^n + t_{\text{end}}) & t_i^n + t_{\text{end}} < t < t_i^n + T \end{cases}$$

$$\Delta_i = \begin{cases} \psi(t_i^n + t_{\text{start}}) - \hat{\psi}_i(t_i^n + t_{\text{start}}) & |\psi(t_i^n + t_{\text{start}}) - \hat{\psi}_i(t_i^n + t_{\text{start}})| < 5^\circ \\ 5^\circ & \text{otherwise} \end{cases}$$

where  $t_{\text{start}}$  and  $t_{\text{end}}$  were set to 40% and 80%, respectively, of the duration of the half elliptical curve of the leg tip trajectory (= 0.12 and 0.23 s) determined experimentally. This controller means that each leg changed its yaw direction toward the target only during the swing phase with  $5^\circ$  of the maximum turning angle for one gait cycle. We also limited the maximum angle of the leg yaw joint to  $5^\circ$  during the turning task. This supplementary control did not aim to make the robot follow the optimal curved path generated by the turning strategy using pitchfork bifurcation. Instead, it was designed so that the first module modulated the walking direction based on the target direction, which solves the problems related

to the feedforward property of the optimal turning strategies and the turning direction due to initial robot conditions, and furthermore allows the robot to approach the target even when  $k_1 \neq \hat{k}_1$ .

#### ACKNOWLEDGMENT

This study was supported in part by JSPS KAKENHI Grant Numbers JP17H04914, JP19KK0377, and JP20H00229; JST FOREST Program Grant Number JPMJFR2021; and the Inamori Foundation.

#### REFERENCES

- [1] Aguilar, J., Zhang, T., Qian, F., Kingsbury, M., McInroe, B., Mazouchova, N., Li, C., Maladen, R., Gong, C., Travers, M., Hatton, R.L., Choset, H., Umbanhowar, P.B. & Goldman, D.I. A review on locomotion robophysics: the study of movement at the intersection of robotics, soft matter and dynamical systems. *Rep. Prog. Phys.* **79**, 110001 (2016).
- [2] Aoi, S., Egi, Y. & Tsuchiya, K. Instability-based mechanism for body undulations in centipede locomotion. *Phys. Rev. E* **87**, 012717 (2013).
- [3] Aoi, S., Tanaka, T., Fujiki, S., Funato, T., Senda, K. & Tsuchiya, K. Advantage of straight walk instability in turning maneuver of multilegged locomotion: a robotics approach. *Sci. Rep.* **6**, 30199 (2016).
- [4] Aoi, S., Manoonpong, P., Ambe, Y., Matsuno, M. & Wörgötter, F. Adaptive control strategies for interlimb coordination in legged robots: A review. *Front. Neurobot.* **11**, 39 (2017).
- [5] Arena, E., Arena, P. & Patanè, L. Efficient hexapodal locomotion control based on flow-invariant subspaces. In *Proc. IFAC World Congress*, pp. 13758-13763 (2011).
- [6] Arm, P., Zenkl, R., Barton, P., Beglinger, L., Dietsche, A., Ferrazzini, L., Hampp, E., Hinder, J., Huber, C., Schaufelberger, D., Schmitt, F., Sun, B., Stolz, B., Kolvenbach, H. & Hutter, M. SpaceBok: A dynamic legged robot for space exploration. In *Proc. IEEE Int. Conf. Robot. Autom.*, pp. 6288-6294 (2019).
- [7] Astley, H.C., Gong, C., Daib, J., Travers, M., Serrano, M.M., Vela, P.A., Choset, H., Mendelson III, J.R., Hu, D.L. & Goldman, D.I. Modulation of orthogonal body waves enables high maneuverability in sidewinding locomotion. *Proc. Natl. Acad. Sci. USA* **112**, 6200-6205 (2015).
- [8] Avanzini, G. & de Matteis, G. Bifurcation analysis of a highly augmented aircraft model. *J. Guid. Contr. Dyn.* **20**, 754-759 (1997).
- [9] Byrd, J.S. & DeVries, K.R. A six-legged telerobot for nuclear applications development. *Int. J. Robot. Res.* **9**, 43-52 (1990).
- [10] Collins, S.H., Ruina, A.L., Tedrake, R. & Wisse, M. Efficient bipedal robots based on passive-dynamic walkers. *Science* **307**, 1082-1085 (2005).
- [11] Courtine, G. & Schieppati, M. Human walking along a curved path. II. Gait features and EMG patterns. *Eur. J. Neurosci.* **18**, 191-205 (2003).
- [12] Cully, A., Clune, J., Tarapore, D. & Mouret, J.-B. Robots that can adapt like animals. *Nature* **521**, 503-507 (2015).
- [13] Curet, O.M., Patankar, N.A., Lauder, G.V. & MacIver, M.A. Aquatic manoeuvring with counter-propagating waves: A novel locomotive strategy. *J. R. Soc. Interface* **8**, 1041-1050 (2011).
- [14] Degraeve, J., Burm, M., Waegeman, T., Wyffels, F. & Schrauwen, B. Comparing trotting and turning strategies on the quadrupedal oncilla robot. In *Proc. IEEE Int. Conf. Robot. Biomim.*, pp. 228-233 (2013).
- [15] Dickinson, M.H., Farley, C.T., Full, R.J., Koehl, M.A.R., Kram, R. & Lehman, S. How animals move: An integrative view. *Science* **288**, 100-106 (2000).
- [16] Fish, F.E., Hurley, J. & Costa, D.P. Maneuverability by the sea lion *Zalophus californianus*: turning performance of an unstable body design. *J. Exp. Biol.* **206**, 667-674 (2003).
- [17] Fish, F.E. Balancing requirements for stability and maneuverability in cetaceans. *Integr. Comp. Biol.* **42**, 85-93 (2002).
- [18] Full, R.J., Kubow, T., Schmitt, J., Holmes, P. & Koditschek, D. Quantifying dynamic stability and maneuverability in legged locomotion. *Integr. Comp. Biol.* **42**, 149-157 (2002).
- [19] Guckenheimer, J. & Holmes, P. *Nonlinear oscillations, dynamical systems, and bifurcations of vector fields*, Springer-Verlag (2002).
- [20] Hirose, S. A study of design and control of a quadruped walking vehicle. *Int. J. Robot. Res.* **3**, 113-133 (1984).
- [21] Hoffman, K.L. & Wood, R.J. Myriapod-like ambulation of a segmented microrobot. *Auton. Robot.* **31**, 103-114 (2011).

- [22] Horvat, T., Melo, K. & Ijspeert, A.J. Spine controller for a sprawling posture robot. *IEEE Robot. Autom. Lett.* **2**, 1195-1202 (2017).
- [23] Hwangbo, J., Lee, J., Dosovitskiy, A., Bellicoso, D., Tsounis, V., Koltun, V. & Hutter, M. Learning agile and dynamic motor skills for legged robots. *Sci. Robot.* **4**, eaau5872 (2019).
- [24] Ijspeert, A.J., Crespi, A., Ryzcko, D. & Cabelguen, J.-M. From swimming to walking with a salamander robot driven by a spinal cord model. *Science* **315**, 1416-1420 (2007).
- [25] Ijspeert, A.J. Biorobotics: Using robots to emulate and investigate agile locomotion. *Science* **346**, 196-203 (2014).
- [26] Kuznetsov, Y.A. *Elements of applied bifurcation theory*, Springer-Verlag (2004).
- [27] Kano, T., Sakai, K., Yasui, K., Owaki, D. & Ishiguro, A. Decentralized control mechanism underlying interlimb coordination of millipedes. *Bioinspir. Biomim.* **12**, 036007 (2017).
- [28] Kwatny, H.G., Bennett, W.H. & Berg, J. Regulation of relaxed static stability aircraft. *IEEE Trans. Automat. Contr.* **36**, 1315-1332 (1991).
- [29] Li, C., Umbanhowar, P.B., Komsuoglu, H., Koditschek, D.E. & Goldman, D.I. Sensitive dependence of the motion of a legged robot on granular media. *Proc. Natl. Acad. Sci. USA* **106**, 3029-3034 (2009).
- [30] Li, C., Zhang, T. & Goldman, D.I. A terradynamics of legged locomotion on granular media. *Science* **339**, 1408-1411 (2013).
- [31] Maladen, R.D., Ding, Y., Umbanhowar, P.B., Kamor, A. & Goldman, D.I. Mechanical models of sandfish locomotion reveal principles of high performance subsurface sand-swimming. *J. R. Soc. Interface* **8**, 1332-1345 (2011).
- [32] Manoonpong, P., Parlitz, U. & Wörgötter, F. Neural control and adaptive neural forward models for insect-like, energy-efficient, and adaptable locomotion of walking machines. *Front. Neural Circuits* **7**, 12 (2013).
- [33] Mastalli, C., Havoutis, I., Focchi, M., Caldwell, D.G. & Semini, C. Motion planning for quadrupedal locomotion: Coupled planning, terrain mapping and whole-body control. *IEEE Trans. Robot.* **36**, 1635-1648 (2020).
- [34] Miguel-Blanco, A. & Manoonpong, P. General distributed neural control and sensory adaptation for self-organized locomotion and fast adaptation to damage of walking robots. *Front. Neural Circuits* **14**, 46 (2020).
- [35] Ning, M., Ma, Z., Chen, H., Cao, J., Zhu, C., Liu, Y. & Wang, Y. Design and analysis for a multifunctional rescue robot with four-bar wheel-legged structure. *Adv. Mech. Eng.* **10**, 1-14 (2018).
- [36] Owaki, D. & Ishiguro, A. A quadruped robot exhibiting spontaneous gait transitions from walking to trotting to galloping. *Sci. Rep.* **7**, 277 (2017).
- [37] Park, H-W., Wensing, P.M. & Kim, S. High-speed bounding with the MIT Cheetah 2: Control design and experiments. *Int. J. Robot. Res.* **36**, 167-192 (2017).
- [38] Parsons, M.M., Krapp, H.G. & Laughlin, S.B. Sensor fusion in identified visual interneurons. *Curr. Biol.* **20**, 624-628 (2010).
- [39] Proctor, J. & Holmes, P. Steering by transient destabilization in piecewise-holonomic models of legged locomotion. *Reg. Chaot. Dyn.* **13**, 267-282 (2008).
- [40] Raibert, M., Blankespoor, K., Nelson, G., Playter, R. & BigDog Team BigDog, the rough-terrain quadruped robot. In *Proc. IFAC World Congress*, pp. 10822-10825 (2008).
- [41] Roy, S.S. & Pratihar, D.K. Kinematics, dynamics and power consumption analyses for turning motion of a six-legged robot. *J. Intell. Robot. Syst.* **74**, 663-688 (2014).
- [42] Schmitt, J. & Holmes, P. Mechanical models for insect locomotion: dynamics and stability in the horizontal plane - II. Application. *Biol. Cybern.* **83**, 517-527 (2000).
- [43] Sefati, S., Neveln, I.D., Roth, E., Mitchell, T.R.T., Snyder, J.B., MacIver, M.A., Fortune, E.S. & Cowan, N.J. Mutually opposing forces during locomotion can eliminate the tradeoff between maneuverability and stability. *Proc. Natl. Acad. Sci. USA* **110**, 18798-18803 (2013).
- [44] Spröwitz, A.T., Tuleu, A., Ajallooeian, M., Vespignani, M., Möckel, R., Eckert, P., D'Haene, M., Degraeve, J., Nordmann, A., Schrauwen, B., Steil, J. & Ijspeert, A.J. Oncilla robot: A versatile open-source quadruped research robot with compliant pantograph legs. *Front. Robot. AI* **19**, 67 (2018).
- [45] Stamper, S.A., Sefati, S. & Cowan, N.J. Snake robot uncovers secrets to sidewinders' maneuverability. *Proc. Natl. Acad. Sci. USA* **112**, 5870-5871 (2015).
- [46] Steingrube, S., Timme, M., Wörgötter, F. & Manoonpong, P. Self-organized adaptation of a simple neural circuit enables complex robot behaviour. *Nat. Phys.* **6**, 224-230 (2010).
- [47] Strogatz, S.H. *Nonlinear dynamics and chaos: With applications to physics, biology, chemistry, and engineering*, Perseus Books: New York (1994).
- [48] Takahashi, R. & Inagaki, S. Walk control of segmented multi-legged robot based on integrative control of legs and 2-DoF active intersegment joints. *Adv. Robot.* **30**, 1354-1364 (2016).
- [49] Taylor, G.K. & Krapp, H.G. Sensory systems and flight stability: What do insects measure and why? *Adv. Insect Physiol.* **34**, 231-316 (2007).
- [50] Tsujita, K., Toui, H. & Tsuchiya, K. Dynamic turning control of a quadruped locomotion robot using oscillators. *Adv. Robot.* **19**, 1115-1133 (2005).
- [51] Toshiba corp. Quadruped robot for nuclear facilities, *E-J. Adv. Maint.* **6**, NT64 (2014).
- [52] Vukobratović, M., Borovac, B., Surla, D. & Stokić, D. *Biped locomotion-dynamics, stability, control and application*, Springer-Verlag (1990).
- [53] Webb, P.W. Designs for stability and maneuverability in aquatic vertebrates: What can we learn? In *Proc. Int. Symp. Unman. Unteth. Sub. Tech.*, pp. 86-108 (1997).
- [54] Wei, T., Luo, Q., Mo, Y., Wang, Y. & Cheng, Z. Design of the three-bus control system utilising periodic relay for a centipede-like robot. *Robotica* **34**, 1841-1854 (2016).
- [55] Wilcox, B.H., Litwin, T., Biesiadecki, J., Matthews, J., Heverly, M., Morrison, J., Townsend, J., Ahmad, N., Sirota, A. & Coope, B. Athlete: A cargo handling and manipulation robot for the moon. *J. Field Robot.* **24**, 421-434 (2007).
- [56] Zhao, D. & Revzen, S. Multi-legged steering and slipping with low DoF hexapod robots. *Bioinspir. Biomim.* **15**, 045001 (2020).
- [57] Zhu, Y., Guo, T., Liu, Q., Zhu, Q., Zhao, X. & Jin, B. Turning and radius deviation correction for a hexapod walking robot based on an ant-inspired sensory strategy. *Sensors* **17**, 2710 (2017).